Japanese Journal of Radiology (2019) 37:154–164
https://doi.org/10.1007/s11604-018-0801-9

ORIGINAL ARTICLE

Multidimensional analysis of clinicopathological characteristics of false-negative clinically significant prostate cancers on multiparametric MRI of the prostate in Japanese men

Ayumu Kido[1] · Tsutomu Tamada[1] · Naoki Kanomata[2] · Akira Yamamoto[1] · Yoshiyuki Miyaji[3] · Atsushi Nagai[3] · Teruki Sone[1]

Received: 6 June 2018 / Accepted: 18 July 2018 / Published online: 1 January 2019

Abstract

Purpose To clarify clinicopathological features of false-negative clinically significant prostate cancer (csPC) at multiparametric prostate MRI (mpMRI).

Methods 95 patients with 139 csPC undergoing 3T mpMRI before radical prostatectomy were included. Two radiologists were independently evaluated mpMR images using PI-RADS v2. Clinicopathological findings were compared between (a) detectable and undetectable lesions using overall mpMRI criteria (o-mpMRI criteria) and (b) lesions with early enhancement effect (EEE) and lesions without EEE at DCE-MRI.

Results The detection rate of csPS using cutoff value of category 3 or more in PI-RADS v2 for positive lesion was 72.1% (98/136 lesions). In 38 false-negative lesions with less than PI-RADS v2 category 3, the DCE-MRI detected 14 lesions. 17 undetectable lesions on o-mpMR criteria had lower PSA and D'amico risk classification, and higher tumor apparent diffusion coefficient (ADC) than those of 118 detectable lesions ($p \leq 0.048$). 89 lesions with EEE showed higher PSA, tumor size, prostatectomy GS grade, frequency of lesions with GS $\geq 4+3$ and lower tumor ADC than those in 38 lesions without EEE ($p \leq 0.046$).

Conclusion Tumor detectability of csPC with PI-RADS v2 was limited compared with o-mpMRI criteria in Japanese men. Moreover, false-negative lesions on o-mpMRI criteria were characterized as small in size, low risk and low cellularity.

Keywords Magnetic resonance imaging · Prostate cancer · Tumor detection · Prostate imaging and reporting data system version 2 · Dynamic contrast-enhanced MR imaging

Introduction

It has been reported that about 161,360 new prostate cancer (PC) cases in the United States and 86,100 new PC cases in the Japan were diagnosed in 2017, and the disease is the second and the sixth leading cause of cancer death for men, respectively [1, 2]. PC has been classified as clinically significant (cs) tumor, for which curative therapies such as radical prostatectomy are indicated, and clinically insignificant (ci) tumor, for which active surveillance using serum prostate-specific antigen (PSA) is indicated [3, 4]. Therefore, accurate pre-biopsy evaluation is essential to efficiently discriminate csPC from ciPC among multicentric PCs in each subject.

In recent years, prostate multiparametric magnetic resonance imaging (mpMRI) has become the best diagnostic imaging tool for detecting csPCs [5, 6]. Moreover, in 2015, the Prostate Imaging and Reporting Data System Version 2 (PI-RADS v2) was standardized for the assessment of the probability (PIRADS assessment category) of csPC using prostate mpMRI [3]. As a feature of PI-RADS v2, dynamic contrast-enhanced MRI (DCE-MRI) plays a minor role in mpMRI for determining the PIRADS assessment category [3], because it is said that absence of the early enhancement

✉ Ayumu Kido
a-k.24@med.kawasaki-m.ac.jp

[1] Department of Radiology, Kawasaki Medical School, 577 Matsushima, Kurashiki City, Okayama 701-0192, Japan

[2] Department of Pathology, Kawasaki Medical School, 577 Matsushima, Kurashiki City, Okayama 701-0192, Japan

[3] Department of Urology, Kawasaki Medical School, 577 Matsushima, Kurashiki City, Okayama 701-0192, Japan

effect (EEE) within a lesion usually adds little information [3]. That is, this may mean lack of clinical knowledge of the difference between PCs with the EEE and PCs without the EEE. On the other hand, PI-RADS v2 shows a higher rate of false-negative results for csPC detection within the low PI-RADS assessment category [7–12]. In addition, in usual clinical practice, we often see csPCs with a false-negative result showing a low PI-RADS assessment category that could detect the lesion using the conventional overall assessment using mpMRI including T2-weighted fast spin-echo (FSE) imaging (T2WI), diffusion-weighted imaging (DWI), and DCE-MRI, not PI-RADS v2. On the other hand, a fraction of csPCs that are not detected by the overall assessment using mpMRI also exist; that is, they are undetectable by all three sequences [6, 13–17]. Only a few previous studies have assessed the clinical and biological differences between detectable and undetectable csPCs on mpMRI including DCE-MRI [15, 16, 18–20]. In particular, the differences between csPCs with the EEE and csPCs without the EEE remain unclear [16]. Accordingly, a multidimensional analysis to understand such characteristics in csPCs showing false-negative results on mpMRI may provide useful information for the next revision of PI-RADS to further improve the diagnostic accuracy of csPC.

Therefore, the aim of this study was to clarify the clinicopathological features of false-negative csPC on mpMRI.

Materials and methods

Patient selection

This single-center retrospective study was approved by the local institutional review board with a waiver of the requirement for written, informed consent.

A total of 100 consecutive patients with biopsy-proven prostate adenocarcinoma who underwent prostate mpMRI followed by radical prostatectomy at our institution were initially identified. Then, 143 PCs with tumor diameter larger than 5 mm and Gleason score (GS) $\geq 3+3$ were identified from detailed diagrams mapping the location of tumors within the prostate at the time of radical prostatectomy. In addition, a lesion with GS ≥ 7 and tumor size ≥ 5 mm or a lesion with GS $= 3+3$ and tumor size ≥ 0.5 mL (tumor size ≥ 8 mm in diameter) was considered a csPC, which was the focus of this study. Of these, 4 PCs with GS $= 3+3$ and tumor size < 0.5 mL were excluded. These exclusions resulted in a final study cohort of 95 patients with 139 PCs (Fig. 1). No patient had undergone any treatment for PC at the time of the prostate MRI examination. The clinicopathological features of the study population are summarized in Table 1.

MRI

After intramuscular administration of buscopan or glucagon to decrease intestinal peristalsis, all MRI examinations were performed under the fasting condition using a 3-T scanner with a 16-channel phased-array coil (Toshiba Medical Systems, Tochigi, Japan).

MRI protocols included axial T1-weighted FSE imaging, axial and coronal T2WI, axial fat-suppressed single-shot echo-planar DWI, and axial DCE-MRI. DWI was acquired with motion-probing gradient (MPG) pulses applied sequentially along three orthogonal orientations following acquisition at b values of 0 and 2000 s/mm^2. ADC maps were reconstructed by calculating the ADC in each pixel of each slice, and the ADC values were calculated by a mono-exponential fitting for a pair of b values (0 and 2000 s/mm^2). Data acquisition for DCE-MRI began simultaneously with the start of intravenous injection of a gadolinium-based contrast medium of 0.1 mmol/kg body weight at a rate of 3 mL/s [meglumine gadoterate (Magnescope; Guerbet Japan, Tokyo, Japan) or gadopentetate dimeglumine (Magnevist; Bayer Schering Pharma, Osaka, Japan)] or 1.5 mL/s [gadobutrol (Gadovist; Bayer Schering Pharma)] via a power injector, followed by a 40 mL saline flush at the same rate as contrast medium injection. Multiphase DCE-MRI images were obtained every 30 s for 180 s (six phases) in 65 patients with 94 lesions or every 7 s for 210 s (30 phases) in 23 patients with 33 lesions without breath-holding. T2WI and DWI were acquired in all 95 patients with 139 lesions, while DCE-MRI was performed in 88 patients with 127 lesions (Fig. 1). The detailed technical parameters of the mpMRI pulse sequences are shown in Table 2.

Histopathologic examination

The radical prostatectomy specimens underwent standard step sections at 4–6 mm intervals, with subsequent hematoxylin–eosin staining. A uropathologist with 22 years of experience who was blinded to the MRI findings recorded tumor location, tumor diameter, and the GS of all tumor foci, and the locations of extraprostatic extension (EPE) on a standardized diagram of the prostate. EPE was defined histopathologically as the presence of cancer cells beyond the prostatic capsular margin, extending into the periprostatic adipose tissue [21]. The GS of each tumor was evaluated according to the 2014 International Society of Urological Pathology Modified Gleason Grading System [22].

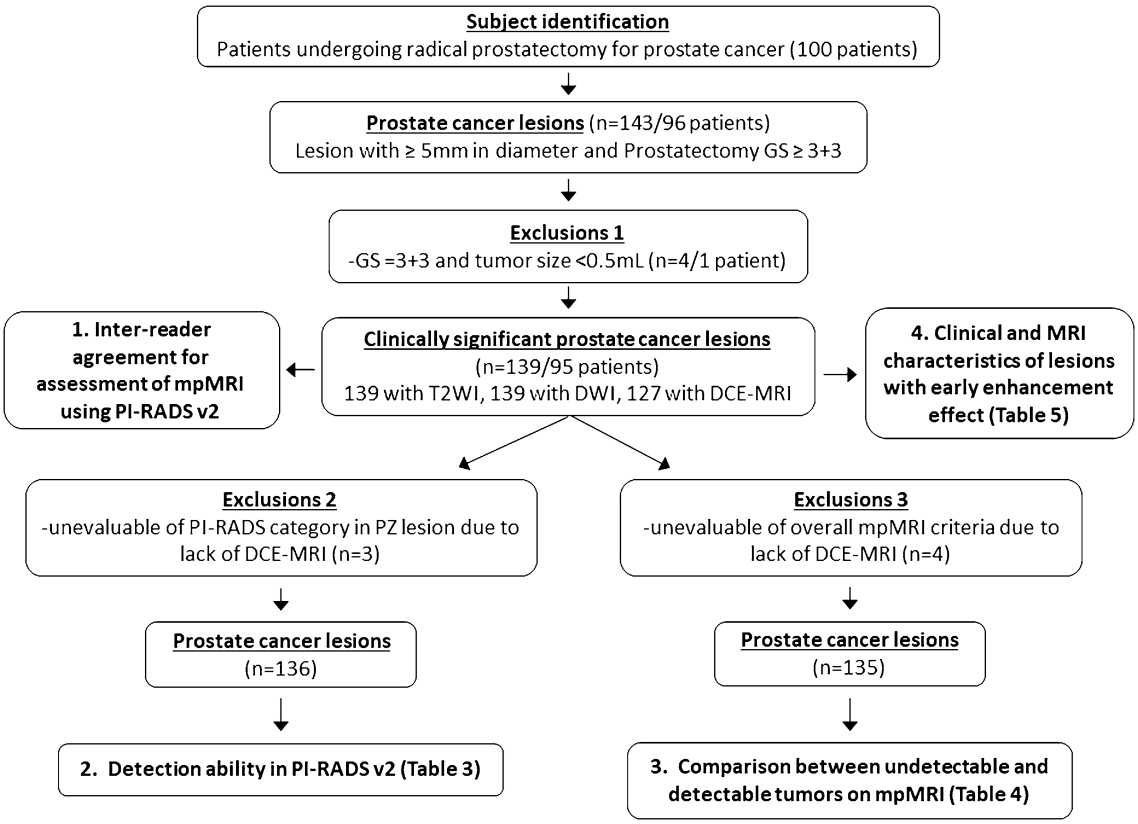

Fig. 1 Patient selection flowchart. *GS* Gleason score, *PI-RADS v2* prostate imaging and reporting data system version 2, *T2WI* T2-weighted imaging, *DWI* diffusion-weighted imaging, *DCE-MRI* dynamic contrast-enhanced MRI, *PZ* peripheral zone

Image analysis and data collection

Two blinded radiologists (A.K. and T.T., with fellowship-trained abdominal radiologists with 5 and 19 years of experience in prostate MRI) and the same uropathologist reviewed all MRI examinations in conjunction with the standardized diagrams of the prostate and determined the location of each tumor indicated by histopathology on multiparametric MRI, mainly T2WI. If a tumor was indistinct on T2WI, DWI and DCE-MRI were used to localize the lesion. This matching was performed by taking into account the tumor size and overall position in the craniocaudal, anteroposterior, and left–right planes on both the MR images and pathologic maps.

The same two radiologists independently assessed the mpMRI of each tumor using PI-RADS v2. These radiologists had 2 years of experience in image interpretation using PI-RADS v2 prior to this study. Each radiologist assigned each tumor a score of 1–5 for T2WI, a score of 1–5 for DWI, positive or negative for DCE-MRI, and the overall PI-RADS assessment category according to PI-RADS v2 [3]. Next, the reviewers reassessed in consensus the mpMRI of tumors for which the score of each sequence and PI-RADS assessment category were discrepant for a given outcome and they determined the final score of the three sequences and the final PI-RADS assessment category. In addition, on DCE-MRI, the degree of the EEE to 90 s after contrast medium administration in each tumor was classified as none (score 0), weak (score 1), moderate (score 2), or strong (score 3) enhancement using a four-point scale. Furthermore, the reviewers determined the presence or absence of EPE according to previously described criteria [23]. These consensus data including the T2WI score, DWI score, positive or negative for DCE-MRI, and EEE score on DCE-MRI were used to determine the final overall PI-RADS assessment category and the overall mpMRI criteria. For tumor detection using the final overall PI-RADS assessment category after consensus reading, categories 1 and 2 were considered negative, and categories 3, 4, and 5 were considered positive. For tumor detection using the overall mpMRI criteria, if each tumor showed positive findings (score 4 or 5 on T2WI, score 4 or 5 on DWI, and EEE score 2 or 3 on DCE-MRI in consensus data mentioned above) on at least one of the three MRI sequences including T2WI, DWI, and DCE-MRI, the lesion was classified as detectable tumor [24]. The remaining lesions were classified as undetectable tumors. The ADC of each tumor was also measured using the region of interest (ROI) placement technique for

Table 1 Clinicopathological characteristics of 95 patients with 139 prostate cancers

Item	Value
No. of patients	95
No. of prostate cancers	139
Age	
Median	69
Range	53–84
Initial PSA level (ng/mL)	
Median	7.83
Range	1.20–38.17
Prostatectomy gleason score	
Median	7
Score (no. of patients)	
3 + 3	8
3 + 3 + 4	5
3 + 4	41
3 + 4 + 5	2
3 + 5	1
4 + 3	27
4 + 3 + 5	4
4 + 4	3
4 + 5	4
Pathological tumor stage (no. of patients)	
T2a	3
T2b	0
T2c	59
T3a	25
T3b	8
D'Amico risk classification (no. of patients)	
Low	4
Intermediate	42
High	49
Lymph node metastasis present (no. of patients)	1
Distant metastasis present (no. of patients)	0

Data are in 95 patients with histologically proved prostate cancer (adenocarcinoma) by prostatic resection

the ADC map by the same two radiologists by consensus. Each ROI was a circle or oval and was chosen to be as large as possible. The volume and mean ADC value of each ROI were recorded.

Clinical data collection

A study coordinator (A.Y.) reviewed the medical and pathology records. Clinical data included age at MRI, initial serum PSA level, prostate volume by preoperative transrectal ultrasound (TRUS), PSA density (ng/mL/cm^3), tumor size, tumor location [PZ, central zone (CZ), and transition zone (TZ)], prostatectomy GS, D'Amico risk classification, and pathological staging (T stage, N stage, and M stage).

Statistical analysis

All statistical tests were performed at the 5% significance level using SPSS for Windows v. 24.0 software (SPSS, Chicago, IL). For the statistical analysis, it was assumed that the multiple lesions per subject were independent. The kappa statistic was used to estimate the inter-reader agreement of the scores for T2WI, DWI, and DCE-MRI and the PI-RADS assessment category between two reviewers. Kappa values of less than 0.20 indicated poor agreement, 0.21–0.40 indicated fair agreement, 0.41–0.60 indicated moderate agreement, 0.61–0.80 indicated good agreement and 0.81 or higher indicated excellent agreement. The clinical and MRI characteristics were compared (a) between undetectable PCs on overall mpMRI criteria and detectable PCs on overall mpMRI criteria and (b) between undetectable PCs on DCE-MRI (EEE score 0 or 1) and detectable PCs on DCE-MRI (EEE score 2 or 3) using Fisher's exact test, the χ^2 test, and the Mann–Whitney *U* test, as appropriate. Age, PSA level, PSA density, prostate volume on TRUS, tumor size, prostatectomy GS grade (GS = 3 + 3, grade 1; GS = 3 + 4, grade 2; GS = 4 + 3, grade 3; GS = 3 + 5, grade 4; GS = 4 + 4, grade 5; GS = 4 + 5, grade 6), D'Amico risk classification (low = 1, intermediate = 2, high = 3), tumor ADC, ROI size on tumor ADC measurement, T2WI score, DWI score, and overall PI-RADS assessment category were compared using the Mann–Whitney *U* test. The frequency of tumor location (PZ or TZ), prostatectomy Gleason score 1 (GS = 3 + 3 or GS ≥ 3 + 4), prostatectomy Gleason score 2 (GS ≤ 3 + 4 or GS ≥ 4 + 3), pathological T stage (pT2 or pT3), and suspected EPE (yes or no) were compared using Fisher's exact test or the χ^2 test. A tumor in CZ was included as PZ tumor for the statistical analysis of tumor location. The significance of the difference in the EEE score between tumors with GS = 3 + 3, tumors with GS = 3 + 4, and tumors with GS ≥ 4 + 3 was assessed using the Kruskal–Wallis test. If the *p* value from the Kruskal–Wallis test was less than 0.05, pairwise comparisons between groups of two were performed using the Mann–Whitney *U* test.

Results

Inter-reader agreement for assessment of mpMRI using PI-RADS v2

For inter-reader agreement between two readers, the kappa value was 0.888 for the T2WI score, 0.951 for the DWI score, 0.929 for the DCE-MRI score, and 0.960 for the

Table 2 Multiparametric MRI sequences and parameters

Sequence	T1-weighted FSE	T2-weighted FSE	T2-weighted FSE	DWI (single-shot SE EPI)	DCE-MRI (3D GRE)	DCE-MRI (3D GRE)
Plane	Axial	Axial	Coronal	Axial	Axial	Axial
TR/TE (ms)	870/12	4300/120	5000/120	7100/95	5.5/2.5	4.0/1.3
Echo train length	4	19	19	NA	NA	NA
Flip angle (degrees)	NA	NA	NA	90	13	12
b values (s/mm^2)	NA	NA	NA	0 and 2000	NA	NA
Field of view (cm)	24×24	24×24	24×24	36×36	35×35	35×28
Matrix size	320×256	384×384	512×192	128×256	320×192	192×144
No. of excitation	1	4	1	3	1	1
Slices thickness (mm)	3	3	3	4	3	3
Parallel imaging factor	2	1.8	NA	2.5	2	2.3
No. of temporal acquisitions					6	30
Temporal resolution (s)					30	7

TR repetition time, *TE* echo time, *FSE* fast spin-echo, *DWI* diffusion-weighted imaging, *EPI* echo-planar imaging, *DCE-MRI* dynamic contrast-enhanced MR imaging, *GRE* gradient-echo, *NA* not applicable

Table 3 Classification of PI-RADS v2 category with mpMRI of 136 clinically significant prostate cancer lesions in 95 patients

PI-RADS v2 assessment category	Total number of lesions	PZ lesion	TZ lesion	Both PZ and TZ lesion
1	18	10	8	
2	20	8	12	
3	12	1	11	
4	59	48[a]	10	1
5	27	17	8	2

Data are in 136 clinically significant prostatic adenocarcinomas with 95 patients who underwent radical prostatectomy

PI-RADS v2 Prostate Imaging and Reporting Data System Version 2, *mpMRI* multiparametric MRI, *PZ* peripheral zone, *TZ* transition zone

[a]Data include a lesion in central zone

overall PI-RADS assessment category, indicating excellent agreement for all.

Tumor detection ability in prostate cancer using PI-RADS v2

Table 3 demonstrates the results of assessment of mpMRI using PI-RADS v2 in 136 csPCs (95 patients) (Fig. 1). In lesion-based and patient-based analyses using a PI-RADS assessment category cutoff of 3 or more for positive tumor detection on mpMRI, the detection rates were 72.1% (98/136 lesions) and 83.2% (79/95 patients), respectively. In 38 lesions with a PI-RADS assessment category less than 3, 4 lesions (all PZ), 7 lesions (all TZ), and 14 lesions (PZ in 6 and TZ in 8) showed positive MRI findings on T2WI (score 4 or 5), DWI (score 4 or 5), and DCE-MRI (moderate or strong EEE), respectively (Figs. 2 and 3). Among the 38 lesions, two lesions with a DWI score 3 in PZ were not assessed for the overall PI-RADS assessment category due to lack of DCE-MRI. Of the remaining 36 lesions, 22 (PZ in 9 and TZ in 13) (PI-RADS assessment category 1 in 9, category 2 in 13) (61.1%) had a positive MRI finding on at least one of the three MRI sequences. On the other hand, in subgroup analyses using 103 lesions with GS ≥ 3 + 4 (81 patients) and 95 lesions with GS ≥ 3 + 4 and diameter ≥ 8 mm (≥ 0.5 cc) (76 patients), the tumor detection rates were 75.7% (78/103 lesions) and 77.9% (74/95 lesions), respectively.

Clinicopathological features of prostate cancers showing undetectable tumor on mpMRI

The results of the comparisons of clinical, pathological, and MRI characteristics between PCs with detectable tumor (detectable mpMRI group) and with undetectable tumor (undetectable mpMRI group) on overall mpMRI criteria are summarized in Table 4 (Figs. 1 and 4). The PSA, PSA density, and D'Amico risk classification were significantly lower in the undetectable mpMRI group than in the detectable mpMRI group, suggesting lower risk tumor in the undetectable mpMRI group ($p = 0.042$–0.048) (Table 4). In addition, the tumor ADC was significantly higher in the undetectable mpMRI group than in the detectable mpMRI group, suggesting lower cellularity in the undetectable mpMRI group ($p < 0.001$).

Clinicopathological features of prostate cancers with the EEE on DCE-MRI

Table 5 shows the results of the comparisons of clinical, pathological, and MRI characteristics between PCs with

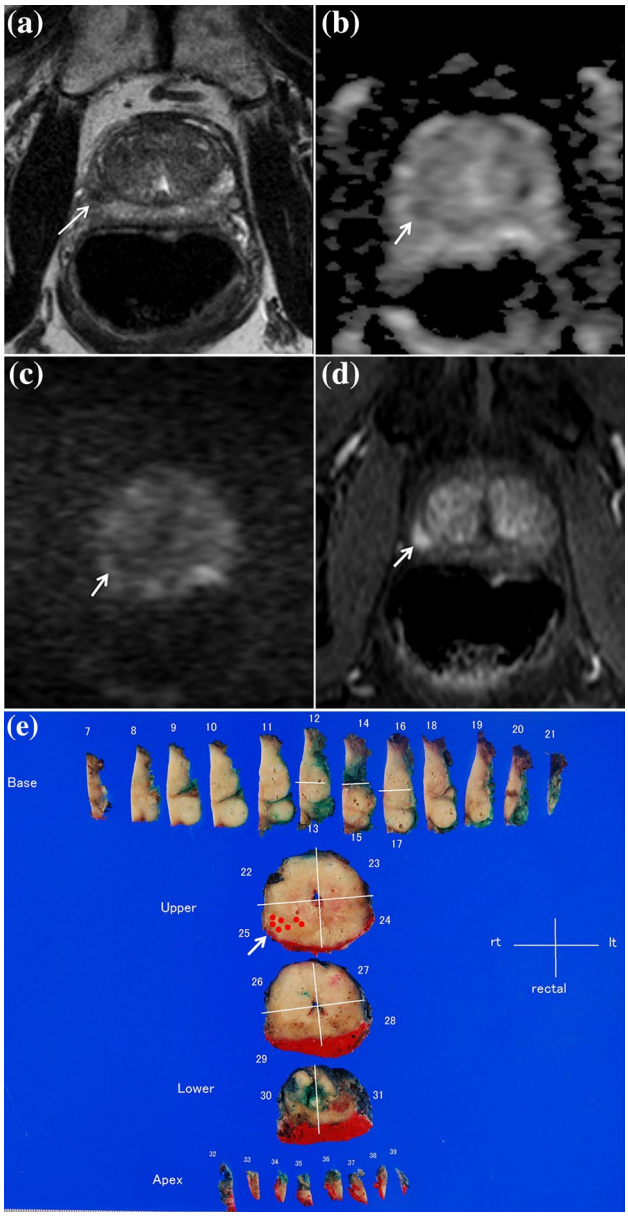

Fig. 2 A 62-year-old man with prostate cancer (prostate-specific antigen level of 6.35 ng/mL, PSA density of 0.13 ng/mL/cm^3) in the middle right region in the peripheral zone (pT2a, pN0, M0, R0, prostatectomy Gleason score of 4 + 5). **a** T2-weighted image shows an area of focal heterogeneous hypointensity with a capsule in the middle right region of the peripheral zone (arrow). **b** Apparent diffusion coefficient (ADC) map shows an indistinct hypointense lesion (arrow). **c** DWI shows isointensity (arrow). **d** Early phase T1-weighted image on DCE-MRI shows focal strong early enhancement (arrow). The lesion was assigned a T2-weighted imaging score of 3, DWI/ADC map score of 2, and DCE-MRI score of positive. The overall category of PI-RADS v2 is 2. **e** Photograph of a macroscopic specimen shows the location of the cancer lesion (arrow)

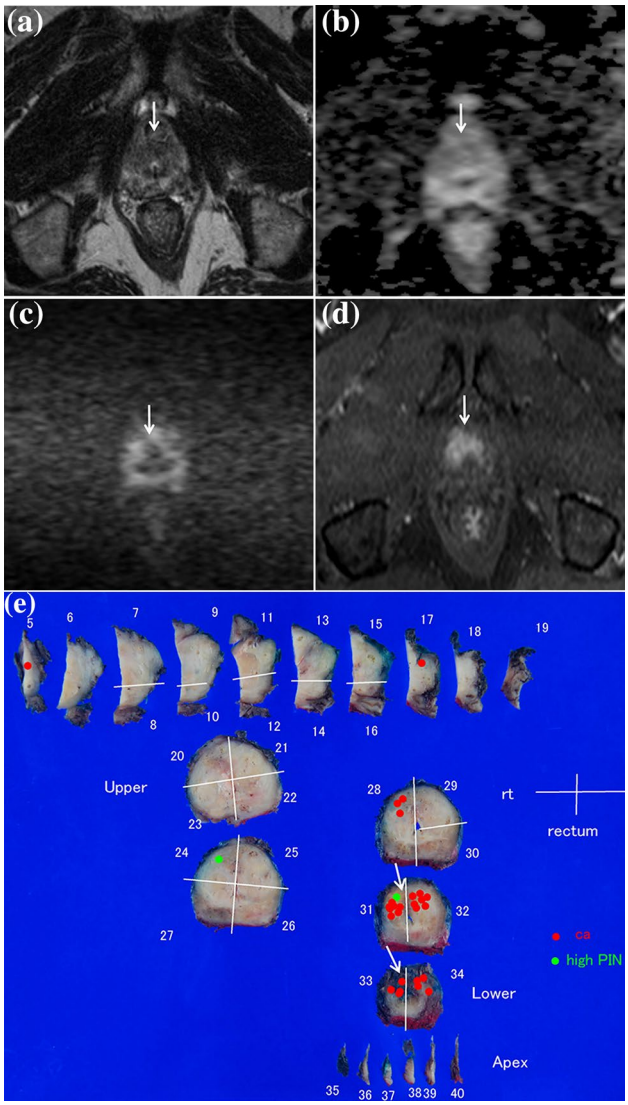

Fig. 3 A 70-year-old man with prostate cancer (prostate-specific antigen level of 12.4 ng/mL, PSA density of 0.50 ng/mL/cm^3) in the bilateral anterior region in the transition zone. (pT2c, pN0, M0, R0, prostatectomy Gleason score of 4 + 3). **a** T2-weighted image shows an area of heterogeneous hypointensity in the apex region of the transition zone (arrow). **b** Apparent diffusion coefficient (ADC) map shows indistinct hypointensity (arrow). **c** No abnormal signal intensity is observed on DWI (arrow). **d** Early phase T1-weighted image on DCE-MRI shows focal moderate early enhancement (arrow). The lesion was assigned a T2-weighted imaging score of 2, DWI/ADC map score of 2, and DCE-MRI score of positive. By PI-RADS v2 decision rules, the overall category is 2. **e** Photograph of a macroscopic specimen shows the location of the cancer lesion (arrow)

(early enhancement group) and without (no early enhancement group) the EEE on DCE-MRI in 88 patients with 127 lesions (Fig. 1). In comparisons between the groups, there were significant differences in the PSA, tumor size, mean prostatectomy GS grade, prostatectomy GS 2 (GS ≤ 3 + 4 vs. GS ≥ 4 + 3), and tumor ADC ($p = 0.001$–0.046), suggesting larger size, more aggressive tumor, such as GS ≥ 4 + 3, and higher cellularity in the early enhancement group. In addition, the T2WI score, DWI score, PI-RADS assessment category, and frequency of suspected EPE were significantly

Table 4 Clinical and MRI characteristics of clinically significant prostatic cancers with undetectable tumors or detectable tumors on prostate multiparametric MRI

Data	Undetectable tumor on mpMRI ($n=17$)	Detectable tumor on mpMRI ($n=118$)	p value
Age (years)[a]	67.1 ± 4.34	68.6 ± 5.59	0.204
PSA (ng/mL)[a]	7.99 ± 4.91	10.6 ± 6.89	0.048
PSA density (ng/mL/cm^3)[a]	0.33 ± 0.22	0.49 ± 0.40	0.045
Prostate volume on TRUS (cm^3)[a]	26.2 ± 7.21	24.7 ± 9.76	0.315
Tumor size (mm)[a]	11.9 ± 4.00	13.9 ± 5.12	0.074
Tumor location[b]			0.364
Peripheral zone	9 (53)	74 (64)	
Transition zone	8 (47)	41 (36)	
Mean prostatectomy Gleason grade[a]	2.00 ± 1.17	2.40 ± 0.99	0.061
Prostatectomy Gleason score 1[b]			0.373
GS = 3 + 3	5 (29)	27 (23)	
GS ≥ 3 + 4	12 (71)	91 (77)	
Prostatectomy Gleason score 2[b]			0.160
GS ≤ 3 + 4	14 (82)	77 (65)	
GS ≥ 4 + 3	3 (18)	41 (35)	
D'Amico risk classification[b]			0.042
Low	2 (12)	4 (4)	
Intermediate	9 (53)	44 (37)	
High	6 (35)	70 (59)	
Pathological T stage[b]			0.217
T2	13 (76)	72 (61)	
T3	4 (24)	46 (39)	
Tumor ADC[a] ($\times 10^{-3}$ mm^2/s)	1.04 ± 0.15	0.76 ± 0.24	< 0.001
Region of interest[a] (mm^2) on tumor ADC measurement	28.4 ± 22.7	30.1 ± 20.2	0.674
Suspected extracapsular extension[b]			0.214
Yes	1 (6)	20 (17)	
No	16 (94)	98 (83)	

Data are in 17 undetectable prostatic adenocarcinomas on mpMRI with 16 patients and 118 detectable prostatic adenocarcinomas on mpMRI with 87 patients who underwent radical prostatectomy

mpMRI multiparametric MRI, *PSA* prostate-specific antigen, *TRUS* transrectal ultrasound, *ADC* apparent diffusion coefficient

[a]Data are the mean ± standard deviation

[b]Numbers in parentheses are percentages

higher in the early enhancement group than in the no early enhancement group, suggesting that tumors with the EEE were easy to detect on T2WI and DWI ($p < 0.001$–0.034). The EEE score was significantly greater for tumors with GS ≥ 4 + 3 than for tumors with GS = 3 + 3 and tumors with GS = 3 + 4 ($p = 0.003$ and 0.022, respectively), but no significant difference between tumors with GS = 3 + 3 and tumors with GS = 3 + 4 ($p = 0.437$) (Table 6).

Discussion

First, the ability of PI-RADS v2 to detect csPC was evaluated using radical prostatectomy as the reference standard. The false-negative rate was 27.9% on a per-lesion basis. However, the use of overall mpMRI criteria detected 61.1% (22/36 lesions) of lesions with a false-negative result (PI-RADS assessment category 1 or 2). In particular, DCE-MRI, which has a minor role for the determination of the PI-RADS v2 assessment category, led to a positive result for more false-negative lesions than T2WI and DWI [3]. Therefore, the present results showed that further revision of PI-RADS including re-evaluation of DCE-MRI is warranted to improve the diagnostic accuracy for the detection of csPCs [11]. In addition, the remaining 14 lesions were not detected (10.1%; 14/139 lesions) even with these assessments. Therefore, particularly on initial prostate biopsy, in addition to MRI-ultrasound fusion targeted prostate biopsy for lesions with highly suspicious mpMRI, conventional systematic biopsy for lesions that

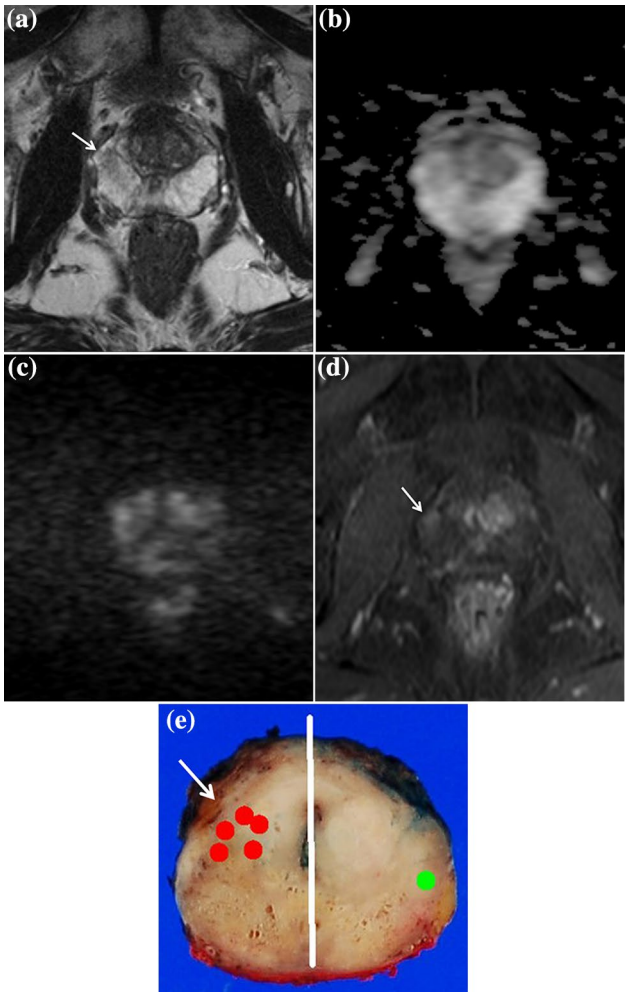

Fig. 4 A 66-year-old man with prostate cancer (prostate-specific antigen level of 4.25 ng/mL, PSA density of 0.18 ng/mL/cm^3) in the middle right region of the peripheral zone (pT2a, pN0, M0, R0, prostatectomy Gleason score of 3 + 3). **a** T2-weighted image shows an area of diffuse slightly low signal intensity in the middle right region of the peripheral zone (arrow). **b**, **c** No abnormal signal intensity is observed on the apparent diffusion coefficient (ADC) map and DWI. **d** Early phase T1-weighted image on DCE-MRI shows no focal early enhancement. The lesion was assigned a T2-weighted imaging score of 2, DWI/ADC map score of 1, and DCE-MRI score of negative. By PI-RADS v2 decision rules, the overall category is 1. **e** Photograph of a macroscopic specimen shows the location of the cancer lesion (arrow)

are undetectable on either mpMRI sequence will need to be performed for reliable detection of csPCs [25–27]. On the other hand, the false-negative rate for the detection of csPCs using PI-RADS v2 was higher in the present study than in previous reports (27.9 vs. 2.7% (11/410 lesions [8]) to 9.3% (15/162 lesions [9]). This difference may be the result of differences in the definition of csPC, age of onset, biological aggressiveness, and tumor size in PC between Western countries and Japan [28–31] and the acquisition methods of mpMRI. However, in the subgroup analyses of present study, the false-negative rate decreased by loosening the definition of csPC.

Next, the 17 undetectable tumors on overall mpMRI criteria were characterized by relatively low-risk PC, in comparison with the detectable tumors. In addition, the undetectable tumors tended to be small in size and low prostatectomy Gleason grade, with marginally significant differences ($p = 0.074$ and 0.061, respectively) (Table 4). Moreover, the lower cellularity with high tumor ADC values was also an important pathological characteristic of the undetectable tumors, indicating less aggressive PC [32–35]. With respect to tumor ADC using DWI with acquisition at b values of 0 and 2000 s/mm^2 with a 3-T scanner, the mean ADC value of 1.04×10^{-3} mm^2/s in the undetectable tumors was equivalent to that of low-risk cancers with Gleason score ≤ 6, since a previous study presented an ADC cutoff value of 0.92×10^{-3} mm^2/s for differentiating between low-risk cancers with Gleason score ≤ 6 and intermediate or high-risk cancers with Gleason score ≥ 7 [36]. Thus, although these undetectable tumors on mpMRI were classified as csPCs in the present study, an undetectable tumor on mpMRI with such features may be included in the category of ciPC by considering its biologic behavior. Further investigations will need to clarify the pathological and prognostic characteristics of such undetectable tumors on mpMRI to accurately differentiate between csPC and ciPC.

Finally, the tumors with the EEE tended to be larger in size, more aggressive, and detectable lesions even on T2WI and DWI, in comparison with the tumors without the EEE. In these results, interestingly, the difference in the prostatectomy Gleason grade between the groups was associated with the difference in the degree of tumors with GS ≤ 3 + 4 and tumors with GS ≥ 4 + 3, but not between tumors with GS = 3 + 3 and tumors with GS ≥ 3 + 4. In addition, there was a significant difference in the degree of the EEE between low-risk (GS = 3 + 3) or intermediate-risk tumor (GS = 3 + 4) and high-risk tumor (GS ≥ 4 + 3). Thus, the neovascularization in PC may develop rapidly at the stage of high-risk tumor. Moreover, past studies showed that discriminating PCs with GS ≤ 3 + 4 from PCs with GS ≥ 4 + 3 is effective for patient prognosis and patient selection for active surveillance [37, 38]. Thus, the EEE on DCE-MRI in addition to tumor ADC, which has high discrimination ability between PCs with GS ≤ 3 + 4 and PCs with GS ≥ 4 + 3, may be a new predictor for determination of risk stratification in PC [28, 34].

There are several limitations in this study. First, it was performed retrospectively in a single institution with a relatively limited sample size. Second, this study included only patients who underwent radical prostatectomy, suggesting patient selection bias. Third, we had two different kinds of multiphase DCE-MR sequences. Thus, the difference might have been influenced for assessment of DCE-MRI. Forth,

Table 5 Clinical and MRI characteristics of clinically significant prostatic cancers with the early enhancement effect or without the early enhancement effect on dynamic contrast-enhanced MRI

Data	Tumor without early enhancement effect on DCE-MRI ($n=38$)	Tumor with early enhancement effect on DCE-MRI ($n=89$)	p value
Age (years)[a]	68.0 ± 3.89	68.6 ± 5.59	0.418
PSA (ng/mL)[a]	8.40 ± 5.71	10.9 ± 6.96	0.031
PSA density (ng/mL/cm^3)[a]	0.35 ± 0.19	0.51 ± 0.42	0.059
Prostate volume on TRUS (cm^3)[a]	24.4 ± 7.28	25.1 ± 9.97	0.963
Tumor size (mm)[a]	12.4 ± 4.63	14.4 ± 5.20	0.015
Tumor location[b]			0.908
Peripheral zone	23 (61)	53 (62)	
Transition zone	15 (39)	33 (38)	
Mean prostatectomy Gleason grade[a]	2.03 ± 1.08	2.34 ± 1.11	0.017
Prostatectomy Gleason score 1[b]			0.219
GS = 3 + 3	12 (32)	19 (21)	
GS ≥ 3 + 4	26 (68)	70 (79)	
Prostatectomy Gleason score 2[b]			0.046
GS ≤ 3 + 4	30 (79)	54 (61)	
GS ≥ 4 + 3	8 (21)	35 (39)	
D'Amico risk classification[b]			0.166
Low	3 (8)	3 (3)	
Intermediate	17 (45)	33 (37)	
High	18 (47)	53 (60)	
Pathological T stage[b]			0.265
T2	27 (71)	54 (61)	
T3	11 (29)	35 (39)	
Tumor ADC[a] ($\times 10^{-3}$ mm^2/s)	0.90 ± 0.26	0.76 ± 0.24	0.001
Region of interest[a] (mm^2) on tumor ADC measurement	26.2 ± 18.1	32.2 ± 21.7	0.113
T2-weighted imaging score[a]	2.82 ± 1.11	3.58 ± 1.16	0.001
DWI score[a]	2.89 ± 1.27	3.78 ± 1.07	< 0.001
PI-RADS v2 assessment category[a]	2.66 ± 1.28	3.76 ± 1.16	< 0.001
Suspected extracapsular extension[b]			0.034
Yes	2 (5)	18 (20)	
No	36 (95)	71 (80)	

Data are in 38 undetectable prostatic adenocarcinomas on DCE-MRI with 30 patients and 89 detectable prostatic adenocarcinomas on DCE-MRI with 71 patients who underwent radical prostatectomy

DCE-MRI dynamic contrast-enhanced MRI, *PSA* prostate-specific antigen, *TRUS* transrectal ultrasound, *ADC* apparent diffusion coefficient, *DWI* diffusion-weighted imaging, *PI-RADS v2* Prostate Imaging and Reporting Data System Version 2

[a]Data are the mean ± standard deviation

[b]Numbers in parentheses are percentages

only pathologically true-positive lesions were used for csPC in this study. Therefore, diagnostic ability such as detection specificity and ROC analysis could not be assessed. Finally, detailed pathological assessments, such as of the epithelium, stroma, and luminal space to clarify biologic features in false-negative csPCs on mpMRI, were not performed in the present study.

In conclusion, tumor detectability of csPC with PI-RADS v2 was limited compared with overall mpMRI criteria in Japanese men. Moreover, false-negative lesions on overall mpMRI criteria were characterized as small in size, low-risk, and low cellularity. These observations demonstrate that further modification of PI-RADS is warranted to improve the detectability of csPCs. DCE-MRI may become a predictor of tumor aggressiveness in PC.

Table 6 Comparison of the degree of the early enhancement effect on dynamic contrast-enhanced MRI among three Gleason score groups

	GS = 3 + 3 (n = 31)	GS = 3 + 4 (n = 53)	GS ≥ 4 + 3 (n = 43)	p value at Kruskal–Wallis test
EEE score[a]	1.74 ± 0.18[†]	1.89 ± 0.16[‡]	2.40 ± 0.13	0.01

Data are in 31 prostatic adenocarcinomas with GS = 3 + 3, 53 prostatic adenocarcinomas with GS = 3 + 4, and 43 prostatic adenocarcinomas with GS ≥ 4 + 3 in 88 patients who underwent radical prostatectomy

EEE early enhancement effect, *GS* Gleason score

[a]Data are the mean ± standard deviation

[†]Significantly different from the GS ≥ 4 + 3 at p = 0.003

[‡]Significantly different from the GS ≥ 4 + 3 at p = 0.022

Acknowledgements This study was supported by the Kawasaki Medical School Project; Contract Grant Number: 29B-044.

Compliance with ethical standards

Conflict of interest The authors have no conflicts of interests to disclose.

Ethical statement This single-center retrospective study was approved by the local institutional review board with a waiver of the requirement for written, informed consent.

References

1. American Cancer Society. Cancer facts and figures 2017. https://www.cancer.org/content/dam/cancer-org/research/cancer-facts-and-statistics/annual-cancer-facts-and-figures/2017/cancer-facts-and-figures-2017.pdf#search=%271.+American+Cancer+Society+%282017%29+Cancer+facts+and+figures+2017.%27. Accessed 29 March 2018.
2. Center for Cancer Control and Information Services, National Cancer Center Japan. Projected Cancer Statistics, 2017. https://ganjoho.jp/en/public/statistics/short_pred.html. Accessed 28 March 2018.
3. Weinreb JC, Barentsz JO, Choyke PL, Cornud F, Haider MA, Macura KJ, et al. PI-RADS prostate imaging—reporting and data system: 2015, Version 2. Eur Urol. 2016;69:16–40.
4. Mottet N, Bellmunt J, Bolla M, Briers E, Cumberbatch MG, De Santis M, et al. EAU-ESTRO-SIOG guidelines on prostate cancer. Part 1: screening, diagnosis, and local treatment with curative intent. Eur Urol. 2016;71:618–29.
5. Hoeks CM, Barentsz JO, Hambrock T, Yakar D, Somford DM, Heijmink SW, et al. Prostate cancer: multiparametric MR imaging for detection, localization, and staging. Radiology. 2011;261:46–66.
6. Ahmed HU, El-Shater Bosaily A, Brown LC, Gabe R, Kaplan R, Parmar MK, et al. Diagnostic accuracy of multi-parametric MRI and TRUS biopsy in prostate cancer (PROMIS): a paired validating confirmatory study. Lancet. 2017;389:815–22.
7. Auer T, Edlinger M, Bektic J, Nagele U, Herrmann T, Schäfer G, et al. Performance of PI-RADS version 1 versus version 2 regarding the relation with histopathological results. World J Urol. 2017;35:687–93.
8. Greer MD, Shih JH, Lay N, Barrett T, Kayat Bittencourt L, Borofsky S, et al. Validation of the dominant sequence paradigm and role of dynamic contrast-enhanced imaging in PI-RADS version 2. Radiology. 2017;285:859–69.
9. Borofsky S, George AK, Gaur S, Bernardo M, Greer MD, Mertan FV, et al. What are we missing? False-negative cancers at multiparametric MR imaging of the prostate. Radiology. 2018;286:186–95.
10. Seo JW, Shin SJ, Taik OhY, Jung DC, Cho NH, Choi YD, et al. PI-RADS version 2: detection of clinically significant cancer in patients with biopsy gleason score 6 prostate cancer. AJR Am J Roentgenol. 2017;209:W1–9.
11. Rosenkrantz AB, Babb JS, Taneja SS, Ream JM. Proposed adjustments to PI-RADS version 2 decision rules: impact on prostate cancer detection. Radiology. 2017;283:119–29.
12. Park SY, Jung DC, Oh YT, Cho NH, Choi YD, Rha KH, et al. Prostate cancer: PI-RADS version 2 helps preoperatively predict clinically significant cancers. Radiology. 2016;280:108–16.
13. Fütterer JJ, Briganti A, De Visschere P, Emberton M, Giannarini G, Kirkham A, et al. Can clinically significant prostate cancer be detected with multiparametric magnetic resonance imaging? A systematic review of the literature. Eur Urol. 2015;68:1045–53.
14. de Rooij M, Hamoen EH, Fütterer JJ, Barentsz JO, Rovers MM. Accuracy of multiparametric MRI for prostate cancer detection: a meta-analysis. AJR Am J Roentgenol. 2014;202:343–51.
15. Le JD, Tan N, Shkolyar E, Lu DY, Kwan L, Marks LS, et al. Multifocality and prostate cancer detection by multiparametric magnetic resonance imaging: correlation with whole-mount histopathology. Eur Urol. 2015;67:569–76.
16. Rosenkrantz AB, Mendrinos S, Babb JS, Taneja SS. Prostate cancer foci detected on multiparametric magnetic resonance imaging are histologically distinct from those not detected. J Urol. 2012;187:2032–8.
17. Turkbey B, Pinto PA, Mani H, Bernardo M, Pang Y, McKinney YL, et al. Prostate cancer: value of multiparametric MR imaging at 3 T for detection–histopathologic correlation. Radiology. 2010;255:89–99.
18. Tan N, Margolis DJ, Lu DY, King KG, Huang J, Reiter RE, et al. Characteristics of detected and missed prostate cancer foci on 3-T multiparametric MRI using an endorectal coil correlated with whole-mount thin-section histopathology. AJR Am J Roentgenol. 2015;205:W87–92.
19. Truong M, Hollenberg G, Weinberg E, Messing EM, Miyamoto H, Frye TP. Impact of gleason subtype on prostate cancer detection using multiparametric magnetic resonance imaging: correlation with final histopathology. J Urol. 2017;198:316–21.
20. Truong M, Feng C, Hollenberg G, Weinberg E, Messing EM, Miyamoto H, et al. A comprehensive analysis of cribriform morphology on magnetic resonance imaging/ultrasound fusion biopsy correlated with radical prostatectomy specimens. J Urol. 2018;199:106–13.
21. Ohori M, Kattan M, Scardino PT, Wheeler TM. Radical prostatectomy for carcinoma of the prostate. Mod Pathol. 2004;17:349–59.
22. Epstein JI, Egevad L, Amin MB, Delahunt B, Srigley JR, Humphrey PA, Grading Committee. The 2014 International Society of Urological Pathology (ISUP) Consensus Conference on gleason grading of prostatic carcinoma: definition of grading patterns and proposal for a new grading system. Am J Surg Pathol. 2016;40:244–52.
23. Tamada T, Sone T, Kanomata N, Miyaji Y, Kido A, Jo Y, et al. Value of preoperative 3T multiparametric MRI for surgical margin status in patients with prostate cancer. J Magn Reson Imaging. 2016;44:584–93.

24. Tamada T, Sone T, Higashi H, Jo Y, Yamamoto A, Kanki A, et al. Prostate cancer detection in patients with total serum prostate-specific antigen levels of 4–10 ng/mL: diagnostic efficacy of diffusion-weighted imaging, dynamic contrast-enhanced MRI, and T2-weighted imaging. AJR Am J Roentgenol. 2011;197:664–70.
25. Radtke JP, Schwab C, Wolf MB, Freitag MT, Alt CD, Kesch C, et al. Multiparametric magnetic resonance imaging (MRI) and MRI-transrectal ultrasound fusion biopsy for index tumor detection: correlation with radical prostatectomy specimen. Eur Urol. 2016;70:846–53.
26. Boesen L, Nørgaard N, Løgager V, Thomsen HS. Clinical outcome following low suspicion multiparametric prostate magnetic resonance imaging or benign magnetic resonance imaging guided biopsy to detect prostate cancer. J Urol. 2017;198:310–5.
27. Cash H, Günzel K, Maxeiner A, Stephan C, Fischer T, Durmus T, et al. Prostate cancer detection on transrectal ultrasonography-guided random biopsy despite negative real-time magnetic resonance imaging/ultrasonography fusion-guided targeted biopsy: reasons for targeted biopsy failure. BJU Int. 2016;118:35–43.
28. Tamada T, Prabhu V, Li J, Babb JS, Taneja SS, Rosenkrantz AB. Assessment of prostate cancer aggressiveness using apparent diffusion coefficient values: impact of patient race and age. Abdom Radiol (NY). 2017;42:1744–51.
29. Zhou CK, Check DP, Lortet-Tieulent J, Laversanne M, Jemal A, Ferlay J, et al. Prostate cancer incidence in 43 populations worldwide: an analysis of time trends overall and by age group. Int J Cancer. 2016;138:1388–400.
30. Cook LS, Goldoft M, Schwartz SM, Weiss NS. Incidence of adenocarcinoma of the prostate in Asian immigrants to the United States and their descendants. J Urol. 1999;161:152–5.
31. Hsing AW, Tsao L, Devesa SS. International trends and patterns of prostate cancer incidence and mortality. Int J Cancer. 2000;85:60–7.
32. Zelhof B, Pickles M, Liney G, Gibbs P, Rodrigues G, Kraus S, et al. Correlation of diffusion-weighted magnetic resonance data with cellularity in prostate cancer. BJU Int. 2009;103:883–8.
33. De Cobelli F, Ravelli S, Esposito A, Giganti F, Gallina A, Montorsi F, et al. Apparent diffusion coefficient value and ratio as noninvasive potential biomarkers to predict prostate cancer grading: comparison with prostate biopsy and radical prostatectomy specimen. AJR Am J Roentgenol. 2015;204:550–7.
34. Tamada T, Prabhu V, Li J, Babb JS, Taneja SS, Rosenkrantz AB. Prostate cancer: diffusion-weighted MR imaging for detection and assessment of aggressiveness-comparison between conventional and kurtosis models. Radiology. 2017;284:100–8.
35. Tamada T, Dani H, Taneja SS, Rosenkrantz AB. The role of whole-lesion apparent diffusion coefficient analysis for predicting outcomes of prostate cancer patients on active surveillance. Abdom Radiol (NY). 2017;42:2340–5.
36. Tamada T, Kanomata N, Sone T, Jo Y, Miyaji Y, Higashi H, et al. High b value (2,000 s/mm^2) diffusion-weighted magnetic resonance imaging in prostate cancer at 3 Tesla: comparison with 1,000 s/mm^2 for tumor conspicuity and discrimination of aggressiveness. PLoS One. 2014;9:e96619.
37. Klotz L, Zhang L, Lam A, Nam R, Mamedov A, Loblaw A. Clinical results of long-term follow-up of a large, active surveillance cohort with localized prostate cancer. J Clin Oncol. 2010;28:126–31.
38. Bul M, van den Bergh RC, Zhu X, Rannikko A, Vasarainen H, Bangma CH, et al. Outcomes of initially expectantly managed patients with low or intermediate risk screen-detected localized prostate cancer. BJU Int. 2012;110:1672–7.